THE JOURNAL OF PHYSICAL CHEMISTRY A

Article

Cite This: J. Phys. Chem. A 2019, 123, 6113−6122

pubs.acs.org/JPCA

Triplet Excitons in Small Helium Clusters

Published as part of The Journal of Physical Chemistry virtual special issue "Hanna Reisler Festschrift".

Parmeet Nijjar,[‡] Anna I. Krylov, Oleg V. Prezhdo, Andrey F. Vilesov, and Curt Wittig*

Department of Chemistry, University of Southern California, 3620 McClintock Avenue, Los Angeles, California 90089-1062, United States

Supporting Information

ABSTRACT: An electron traveling through liquid helium with sufficient kinetic energy can create a low-lying triplet exciton via inelastic scattering. Accompanying repulsion between the exciton and nearby atoms results in bubble formation. That is not all, however. Repulsion compresses an "incipient He_2* exciton", pushing it into a region where an He_2* moiety commences evolution toward its potential energy minimum. The above picture follows from *ab initio* calculations of the two lowest adiabatic potential energy surfaces for collinear three-atom systems and dynamics studies launched on the lowest adiabat that calculate said surface on the fly. The timescale for launching trajectories toward the He_2* moiety is significantly shorter than the timescale for pushing helium away from the exciton in large systems, making results with three atoms relevant to liquid helium. This explains how He_2* might be created in the aftermath of electron-impact excitation of He*. Interplay between the lowest adiabats is discussed, underscoring the importance of nonadiabatic processes in such systems. Results with eight-atom systems further illustrate the critical role of nonadiabatic transitions.

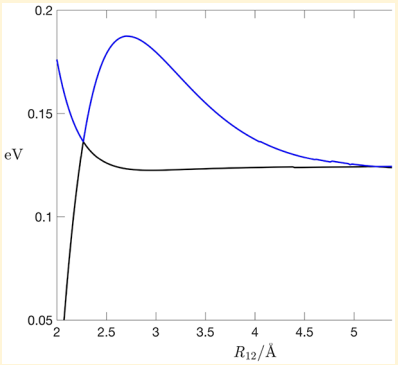

1. INTRODUCTION

An electron traveling through liquid helium with sufficient kinetic energy (eKE) is capable of creating a low-lying electronic excitation via inelastic scattering. When this happens, the excitation is usually localized on an atom or incipient diatom at the moment of its creation. The term "incipient diatom" refers to two atoms that are capable of entering into a stable chemical bond, but whose internuclear separation is so large that the bond is tenuous, *e.g.*, as near the peak of an entrance barrier. An incipient diatom is easily influenced through interactions with its environment. In most cases, stable and metastable electronic excitations in liquid helium have well-understood gas-phase counterparts. Table 1 lists gas-phase species whose energies lie in the range relevant to the present paper.[1−4]

The elastic scattering of an electron in liquid helium lowers its momentum relative to the lab. If inelastic scattering does not intervene, this leads to an electron bubble.[5−10] If inelastic scattering does intervene, bubble formation simply takes less time. Likewise, radiatively metastable triplet atoms and diatomic molecules also form bubbles.[11−14]

Electronically excited diatoms are also produced and removed in the aftermath of inelastic scattering. These processes are often poorly understood.[15−18] For example, one such case motivated the present paper and a previous one.[19] The fates of the inelastically scattered electrons can be interesting. In large nanodroplets, He_n,[20−30] an electron with sufficient eKE can create two or more excited atoms inside the same droplet.[23−25,27,30] We will leave such processes aside, and focus on the fates of liquid-helium counterparts of the lowest excited state of a gas-phase He atom: 1s2s ^{3}S, referred to hereafter as He*. The liquid-helium counterparts are also referred to as He*, the distinction being clear from context.

Table 1. Excited States of Isolated Atomic and Diatomic Helium[a]

species	label	energy/eV
$He(1s2s,^3S)$	He*	19.82
$He(1s2s,^1S)$	$He(2^1S)$	20.62
$He(1s2p,^3P)$	$He(2^3P)$	20.96
$He(1s2p,^1P)$	$He(2^1P)$	21.22
$He_2(a^3\Sigma_u^+)$	He_2*	17.98
$He_2(b^3\Pi_g)$	$b^3\Pi_g$	18.57
$He_2(c^3\Sigma_g^+)$	$c^3\Sigma_g^+$	19.32
$He_2(A^1\Sigma_u^+)$	$A^1\Sigma_u^+$	18.15
$He_2(B^1\Pi_g)$	$B^1\Pi_g$	18.58
$He_2(C^1\Sigma_g)$	$B^1\Sigma_g$	19.50

[a]Energies are relative to separated ground state atoms. Spin−orbit splitting is ignored. Atoms are from the National Institute of Standards and Technology.[1] The $He_2(a^3\Sigma_u^+)$ (He_2*) energy is from D_e calculated by Pavanello *et al.*,[2] with zero point including anharmonicity from Focsa *et al.*[3] The $b^3\Pi_g$ and $c^3\Sigma_g^+$ energies, including zero point with anharmonicity, are from Focsa *et al.*[3] The A-state energy is from Huber and Herzberg.[4] The B and C-state energies, including zero point with anharmonicity, are from Focsa *et al.*[3]

Received: April 8, 2019
Revised: June 2, 2019
Published: July 1, 2019

Downloaded via UNIV OF SOUTHERN CALIFORNIA on April 4, 2020 at 07:14:52 (UTC).
See https://pubs.acs.org/sharingguidelines for options on how to legitimately share published articles.

© 2019 American Chemical Society

DOI: 10.1021/acs.jpca.9b03241
J. Phys. Chem. A 2019, 123, 6113−6122

A He* exciton created by inelastic scattering in liquid helium undergoes dynamical processes following its abrupt birth. Being a Rydberg state, the outermost orbital's electron density extends significantly farther from its nucleus than does the electron density of the ground state atom. Thus, adjacent He atoms experience repulsion concomitantly with He* creation, in which case electron-impact excitation requires more energy than the 19.82 eV of gas-phase He*. The additional energy, ~0.2 eV,[31] though modest compared to 19.82 eV, is important, as it causes significant repulsion near the excitation site. What ensues is He atoms being pushed away from the exciton. This leads eventually to a He* bubble whose radius is about 6 Å.[14] Note that the bubble does not have a smooth periphery, as the average He−He distance of the liquid (3.5 Å, *vide infra*, Figure 5) is too large a percentage of the 6 Å radius. The bubble's interior "surface" must play a role in determining the short 15 μs lifetime of He* in liquid helium.[16,32]

That is not the whole story, however. In addition to the creation of He*, subsequent dynamics yield the triplet diatomic moiety, $He_2(a^3\Sigma_u^+)$.[15] As mentioned above, the lifetime of He* in liquid helium is 15 μs, so at long times $He_2(a^3\Sigma_u^+)$ is the dominant metastable species. We will refer to both gas-phase and condensed-phase $He_2(a^3\Sigma_u^+)$ as He_2*, the distinction being clear from context.

How this species is created remained a puzzle for many years. The gas-phase process, He* + He → He_2*, which is exoergic by ≈2 eV, has a barrier that peaks near 2.7 Å with energy exceeding 500 cm^{-1}. This barrier is formidable at low temperature, to say nothing of the protection afforded by the bubble that hosts He*. We concluded that a He_2* moiety must be formed on a short timescale if He_2* formation is to precede the 15 μs He* lifetime. A preliminary report presented a qualitative model of how this might happen.[19]

Our interest in the conversion of He* to He_2* in liquid helium arose in the context of electron-bombarded large helium nanodroplets whose diameters exceed about 50 nm.[23−25,27,30] It had been shown that a second He_4^+ channel opens when eKE exceeds ≈40 eV.[23,24,27] The He_4^+ ions produced via this channel are formed with high selectivity, and in an electronically excited, radiatively metastable state.[23−25] The $^4A_2$ state was deemed likely (Figure 1).[25,33,34] Fine *et al.* reported delay times of ~10 μs for this channel and pointed out that bubbles harboring He* or He_2* migrate to the surfaces of large droplets, where they roam about and react with one another.[30] In the gas phase, such species react vigorously.[35,36]

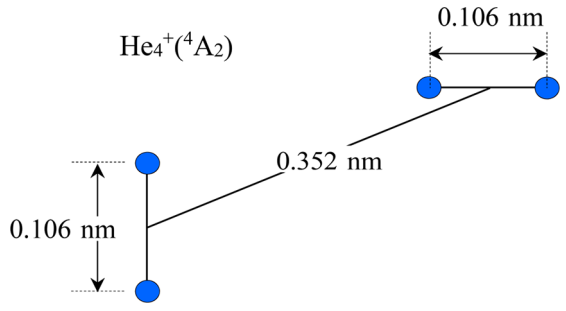

Figure 1. Structure of $He_4^+(^4A_2)$ calculated by Knowles and Murrell.[33,34] Each blue pair is He_2^+. The Rydberg electron is shared between He_2^+ ions. The bond is fairly strong (1.264 eV) despite the large separation between the He_2^+ groups.

The roles of He* and He_2* in the production of He_4^+ has not been established, except to confirm that the 40 eV threshold implicates two He* as the progenitors of radiatively metastable He_4^+.[27] Early studies yielded high-quality data. Intriguing phenomena were discovered, and proposed mechanisms were presented, though not for He_2* production. This work is summarized in ref 19.

Referring to Figure 1, an attractive scenario has two He_2* molecules autoionizing when approaching one another.[33,34] Namely, $He_4^+(^4A_2)$ can be thought of as containing separated He_2^+ ions whose axes are perpendicular to one another and to the line between the He_2^+ centers-of-mass. These ions share the Rydberg electron. To create $He_4^+(^4A_2)$, each He_2* must have ample vibrational energy. This turns out to be the case, *e.g.*, $He_2^*(v = 10-12)$ has been observed spectroscopically.[37]

As mentioned above, electron-impact excitation in liquid helium not only creates an exciton (He* or incipient He_2*) but introduces repulsion between the exciton and nearby He atoms. This repulsion dominates the early time dynamics near the excitation site. However, it can achieve more than merely pushing He atoms away from He*. It applies inward force along the axis of a He*−He pair. When this pair has an internuclear separation near where the entrance barrier peaks (*vide infra*, Figure 6b), it is nudged toward the attractive He_2* potential. That is the crux of the early time dynamics (Figure 2). The present paper presents additional *ab initio* molecular dynamics (AIMD) simulations. It expands on issues raised in ref 19 and introduces new ones.

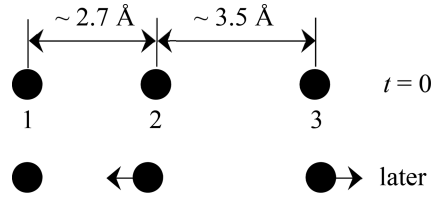

Figure 2. Electron impact promotes He atoms to the lowest triplet. The exciton resides mainly on the left diatom. R_{12} shortens and R_{23} lengthens at early times.

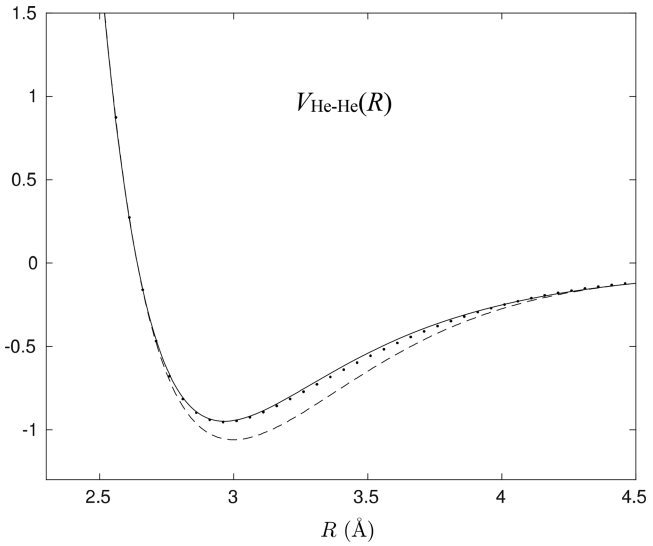

Figure 3. Potential energy curve for two ground state He atoms. Reprinted with permission from ref 38. Copyright 2016 Elsevier. The solid line was calculated at a high level of theory.[39] The dots and dashed line are not relevant here. The energy is in meV.

DOI: 10.1021/acs.jpca.9b03241
J. Phys. Chem. A 2019, 123, 6113−6122

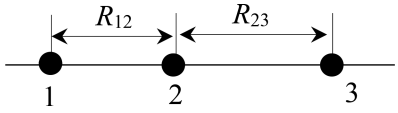

Figure 4. Three He atoms are constrained to a straight line.

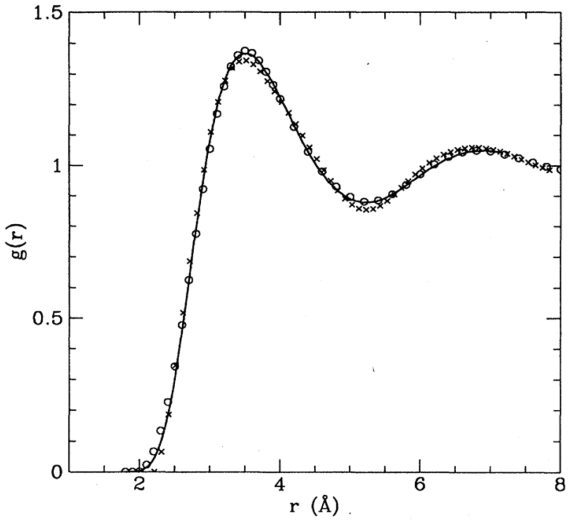

Figure 5. Continuous curve is the calculated radial distribution function for helium at 1.21 K.[55] Points indicate experimental data.[56,57] Reprinted from Figure 16 of ref 55 with permission of the author, D. Ceperley, and APS. Copyright 1995.

The van der Waals (vdW) minimum for two ground state He atoms lies at 2.98 Å with a depth of 8 cm^{-1} (Figure 3), and the pair correlation function $g(r)$ (*vide infra*, Figure 5) describes interatomic spacing in 1.2 K superfluid, with the first (nearest neighbor) peak being at 3.5 Å. Electron-impact excitation samples spacing per $g(r)$. Whereas weak interatomic forces are responsible for the starting configurations at the instant of exciton creation, the dynamics that ensue are influenced by the repulsive forces that accompany the exciton's entry.

In simulations with small helium clusters, the cluster can break apart. There will still be long-range interactions among fragments, but these will be small. In ref 19, we noted that excitons seem to hop over unusually large distances. Indeed, as explained by Li and Tang[40] and by Agronovich[41] such distances are far too large to make sense.[40,41] This artifact is due to the neglect of nonadiabatic transitions. It will be explained below.

We begin with Computational Details, describing the theoretical methods and computational protocols. The Results and Discussion section deals mainly with collinear three-atom systems, explaining the nature of the low-lying manifold adiabatic surfaces and how they participate in the molecular dynamics. A few results with collinear eight-atom systems illustrate energy flow, fragmentation of the original cluster, and a limitation of Born−Oppenheimer dynamics. The central role of nonadiabatic transitions is identified. The Conclusions section is a concise summary.

2. COMPUTATIONAL DETAILS

Calculations were carried out using the Q-Chem electronic structure package.[42,43] Trajectories and orbitals were visualized using IQmol,[44] and natural transition orbitals (NTOs) were plotted using Jmol.[45] Diatomic potential energy curves ($a^3\Sigma_u^+$, $c^3\Sigma_g^+$, and $b^3\Pi_g$) and collinear potential energy surfaces (PESs) were computed using the equation-of-motion for excitation energies coupled-cluster approach with single and double excitations (EOM-EE-CCSD)[46,47] and the doubly augmented Dunning's double-ζ basis set, d-aug-cc-pVDZ. PESs were constructed from excited state energies, with spacing between adjacent atoms incremented by 0.02 Å. Our calculations of diatomic potential energy curves using d-aug-cc-pVDZ and d-aug-cc-pVTZ have shown that differences between results obtained using these bases are not essential. These validation calculations have also confirmed that EOM-EE-CCSD with the d-aug-cc-pVDZ basis gives a good estimate of the excitation energy and barrier height, consistent with earlier results.[14,48]

We analyzed the character of excited states by computing NTOs of EOM-EE-CCSD wave functions at various geometries.[49−51] We also computed NTOs during trajectories to study exciton dynamics. NTOs provide the most compact way to visualize electronic excitations in terms of hole-particle pairs. Representing the electronic transitions in terms of NTOs removes the arbitrariness associated with the choice of molecular orbitals and provides the essential description of the transition. Electron and hole orbitals, $\psi_k^e(r_e)$ and $\psi_k^h(r_h)$, are obtained by singular value decomposition (SVD) of the one-particle transition density matrix. Each pair of hole and particle states is associated with a

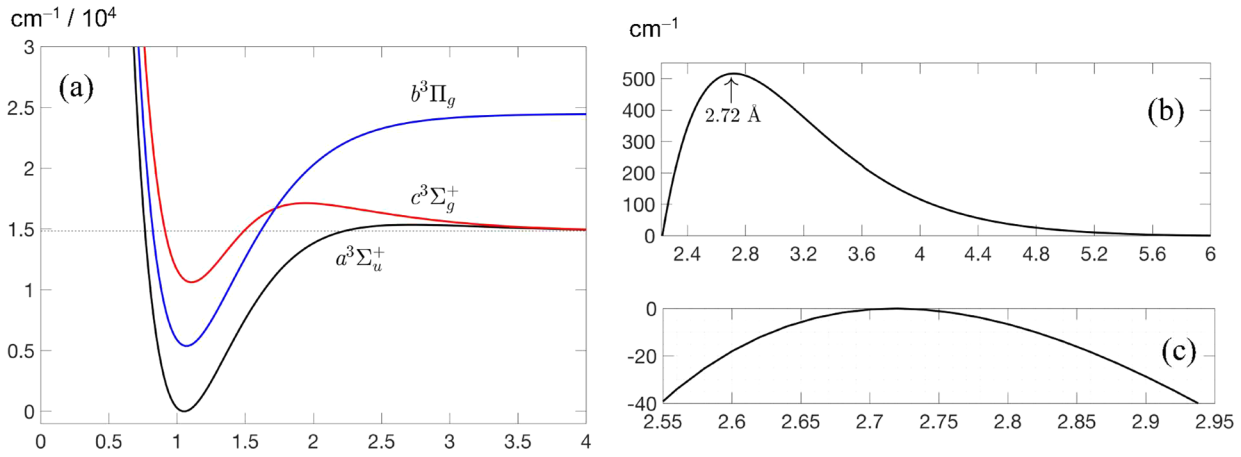

Figure 6. Diatomic potential curves. Horizontal axes are in Å. (a) The $a^3\Sigma_u^+$ minimum is at 1.06 Å. The $a^3\Sigma_u^+$ entrance barrier is barely seen on this energy scale. (b) Expanded view of the barrier; energy is relative to He + He*. The curve crosses E = 0 at 2.24 Å. (c) Further expansion near the peak illustrates the small gradients that facilitate compression of incipient He_2*. Energy is relative to that of the peak at 2.72 Å.

DOI: 10.1021/acs.jpca.9b03241
J. Phys. Chem. A 2019, 123, 6113−6122

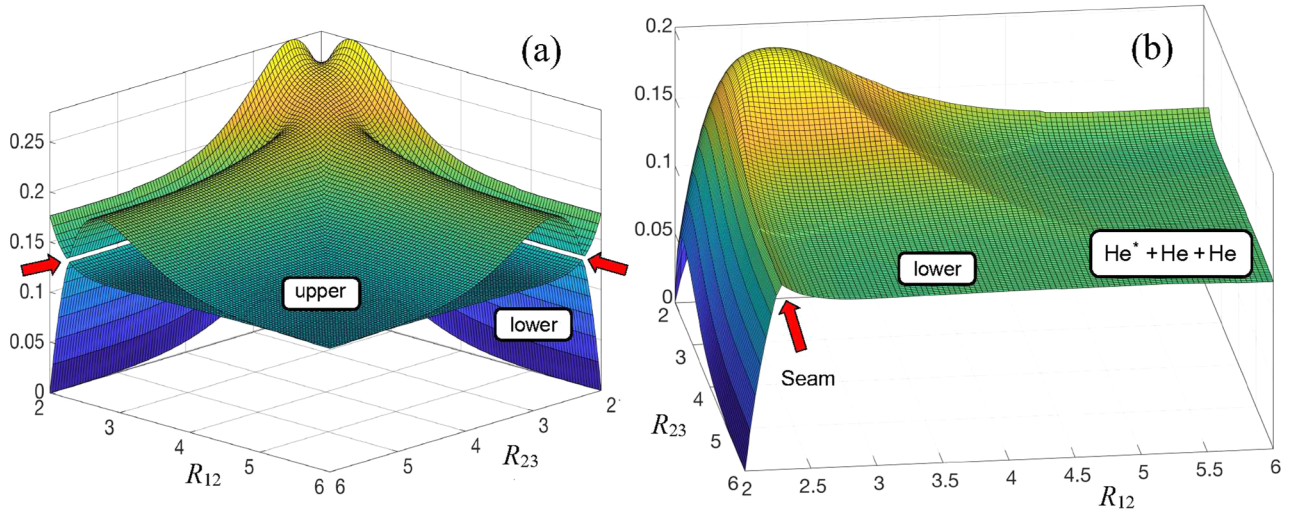

Figure 7. (a) View of the lower and upper adiabats from a distant location with $R_{12} = R_{23}$. Red arrows indicate the near degeneracy. (b) View of the lower adiabat, showing the ridge associated with the near degeneracy (red arrow), and the ridge associated with $R_{12} = R_{23}$. See Supporting Information for other views.

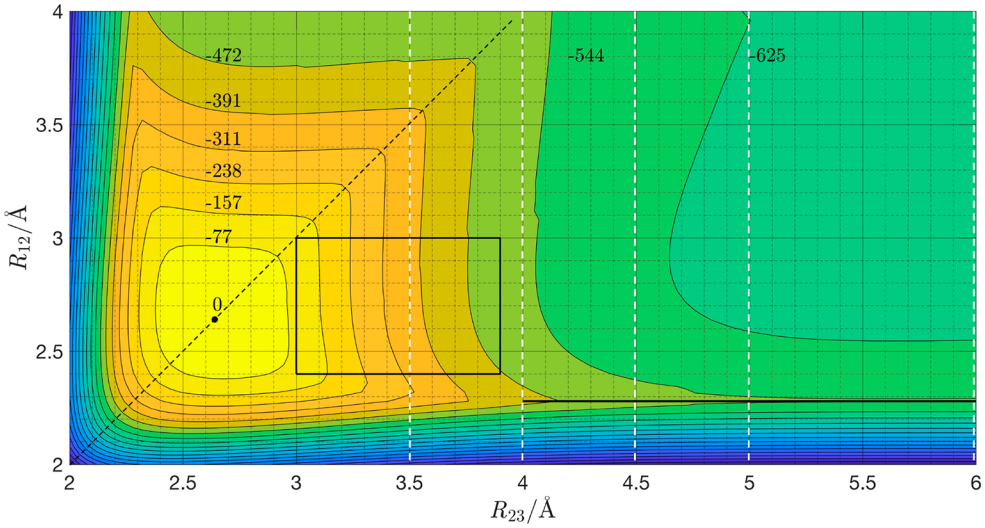

Figure 8. Contour map for the lower adiabat. The near degeneracy is shown as a solid black line between 4.00 and 6.00 Å, where the gaps are 11 and 1.6 cm^{-1}, respectively. Trajectories originate from within and on the rectangle. The dashed white lines at 3.5, 4.0, 4.5, 5.0, and 6.0 Å are where slices were taken (Figure 9 and Supporting Information). The dashed white line at 6.0 Å is offset slightly to the left for visualization. Contour energies are in cm^{-1} relative to the energy at the peak. The figure is symmetric with respect to the black dashed line at 45°.

singular value σ_k, whose square gives the weight of each hole-particle pair in the overall exciton wave function:

$$\chi_{exc}(r_h, r_e) = \sum_k \sigma_k \psi_k^h(r_h)\, \psi_k^e(r_e) \quad (1)$$

where summation runs by all NTO pairs. Usually, a small number of NTO pairs dominate, so excitations can be represented using just one or two electron−hole pairs, facilitating interpretation of excited electronic states. NTO analysis also yields electronic character: valence vs Rydberg; charge-transfer; nn*, nπ*, etc.

We performed AIMD[52] in systems of collinear atoms, with trajectories launched on the lowest triplet state. Excited state energies and gradients were computed at each time-step using EOM-EE-CCSD with the d-aug-cc-pVDZ basis set. Trajectories were propagated for 500 steps (484 fs) with a time-step of 40 atomic units (0.968 fs) using the velocity Verlet algorithm.[53] Simulations were run at constant energy starting from different configurations, each with zero initial kinetic energy.

3. RESULTS AND DISCUSSION

3.1. General Considerations. Detailed studies of collinear three-atom systems (Figure 4) enable insight into early time triplet exciton dynamics in liquid helium. They also reveal that nonadiabatic transitions among low-lying triplet PESs play a central role. A few results with collinear eight-atom systems provide further insight, notably, into nonadiabaticity in such systems.

Classical molecular dynamics cannot describe liquid helium.[54] However, the repulsion that accompanies exciton creation imparts sufficient energy to justify enlistment of the classical domain. Note that a He atom with 100 cm^{-1} of translational energy has a de Broglie wavelength of 1.2 Å. A classical description then becomes appropriate, albeit subject to careful interpretation.

DOI: 10.1021/acs.jpca.9b03241
J. Phys. Chem. A 2019, 123, 6113−6122

Figure 5 shows that the helium radial distribution function $g(r)$ rises sharply near 2.3 Å and peaks at 3.5 Å.[55−57] It gives the distribution of interatomic distances accessible to electron-impact excitation.[58] Our calculated $a^3\Sigma_u^+$ curve (Figure 6) has a barrier whose peak is at 2.72 Å with energy of 516 cm^{-1} relative to He* + He, in accord with high-level theory.[14] We will refer to the analogous exciton in the barrier region as (He−He) * or incipient He_2*, depending on context. Figure 5 shows that separations smaller than 2.7 Å, where the barrier in Figure 6b peaks, account for a small percentage of the nearest neighbors. Launching more trajectories than this toward He_2* requires that exciton creation is accompanied by forces that increase the critical separation, R_{cr}, for which the system commences evolution toward He_2*. Figure 5 enables an estimate of the probability that excitation takes place with at least one nearest neighbor within R_{cr}. This probability is given by $1 - \exp[-4\pi\rho\int_0^{R_{cr}} dr\, r^2 g(r)]$, where ρ is the helium density. Using it, R_{cr} values of 2.5, 2.6, 2.7, 2.8, 2.9, and 3.0 Å yield probabilities of 0.09, 0.15, 0.24, 0.34, 0.45, and 0.57, respectively.

3.2. Collinear Three-Atom Adiabats. Collinear three-atom systems enable the exciton to reside at either an atom or diatom, or to delocalize (to varying degrees) over the three atoms. This manifests in the two lowest energy adiabats, referred to hereafter as the lower and upper adiabats. For example, Figure 7a shows that the $He_2(a^3\Sigma_u^+)$ diatomic potential curve in its barrier region is recovered in the large-R_{23} (equivalently, large R_{12}) limit through a combination of the lower and upper adiabats. Red arrows show where these two adiabats nearly touch. In this case, the exciton resides on the diatom.

Referring to Figure 7a, the lower and upper adiabats nearly touch along lines that run parallel to the axes. Figure 8 shows the near-degeneracy line that runs parallel to the R_{23} axis at R_{12} = 2.27 Å. An equivalent line runs parallel to the R_{12} axis (albeit off-scale in the figure), as the figure is symmetric about a line at 45° to the axes. The small gaps in Figure 7a (red arrows) are due to the grid spacing used to display the surfaces. They almost disappear with a grid whose spacing is not a limiting factor, *i.e.*, dropping to 1.6 cm^{-1} at R_{23} = 6.00 Å and R_{12} = 2.27 Å (equivalently, at R_{12} = 6.00 Å and R_{23} = 2.27 Å).

Figure 9 shows slices through the PESs (see Supporting Information for 4.50 and 5.00 Å). Figure 9a (R_{23} = 6.00 Å) shows that the diatomic He_2* curve follows the lower PES for R_{12} < 2.27 Å (black) and the upper PES for R_{12} > 2.27 Å (blue), with NTOs indicating exciton nature. Each NTO entry shows (top to bottom) the Rydberg orbital, the hole orbital, and the σ_k^2 value. When $\sigma_1^2 \geq 0.90$, just this NTO provides an adequate picture of the exciton. Otherwise, the two leading σ_k^2 values are given.

Orbital composition changes along the He_2* curve. At R_{12} = 2.20 Å (black), bonding and antibonding contributions localized on the R_{12} diatom contribute σ_1^2 = 0.76 and σ_2^2 = 0.20, respectively, whereas at R_{12} = 2.50 Å (blue), their contributions are 0.71 and 0.25. With the exciton on atom 3 there is little change in orbital composition. This curve is the upper PES for R_{12} < 2.27 Å and the lower PES for R_{12} > 2.27 Å, with σ_1^2 values remaining at 0.96 throughout the range shown. The near degeneracy is centered at E = 0.136 eV.

In Figure 9b (R_{23} = 4.00 Å), an 11 cm^{-1} gap is centered at E = 0.149 eV. The NTOs support a picture in which the analog of the He_2* curve is obtained by increasing R_{12} on the lower adiabat, transitioning from lower to upper adiabat at 2.27 Å, and transitioning from upper to lower adiabat at 4.00 Å. Imagine standing to the left of Figure 7b and examining the

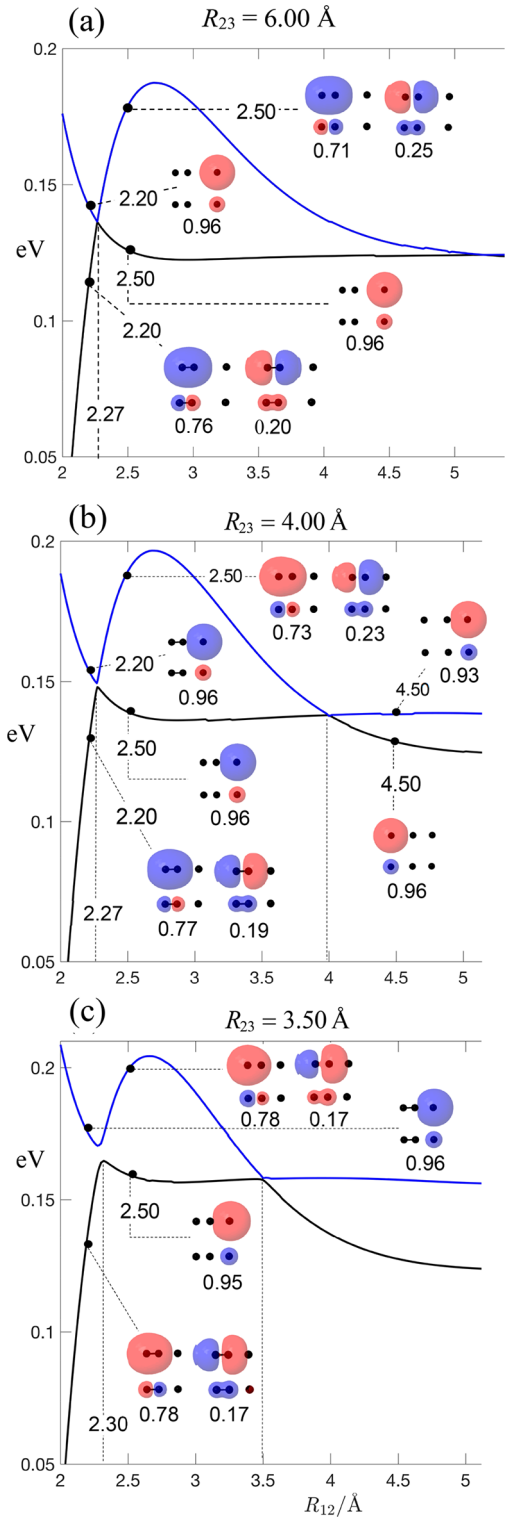

Figure 9. Entries a−c are for progressively smaller R_{23} values (6.00, 4.00, 3.50 Å). Note the red arrows pointing at (R_{12}, R_{23}) = (2.27, 6.00) in Figure 7a. The NTOs show the Rydberg orbital at the top, then the hole, and then the σ_k^2 value. The energy at the near degeneracy increases as R_{23} decreases: 0.136 eV at 6.00 Å; 0.149 eV at 4.00 Å. There is no noticeable change in the value of R_{12} at the near degeneracy (2.27 Å) for $R_{23} \geq$ 4.00 Å. For the slice at R_{23} = 3.50, the gap is at 48 cm^{-1}, the center of the gap is at 0.168 eV, and R_{12} = at the center of the gap is 2.30 eV. Energies are in electronvolts relative to an arbitrary reference energy that is the same in each entry; distances are in Å.

DOI: 10.1021/acs.jpca.9b03241
J. Phys. Chem. A 2019, 123, 6113−6122

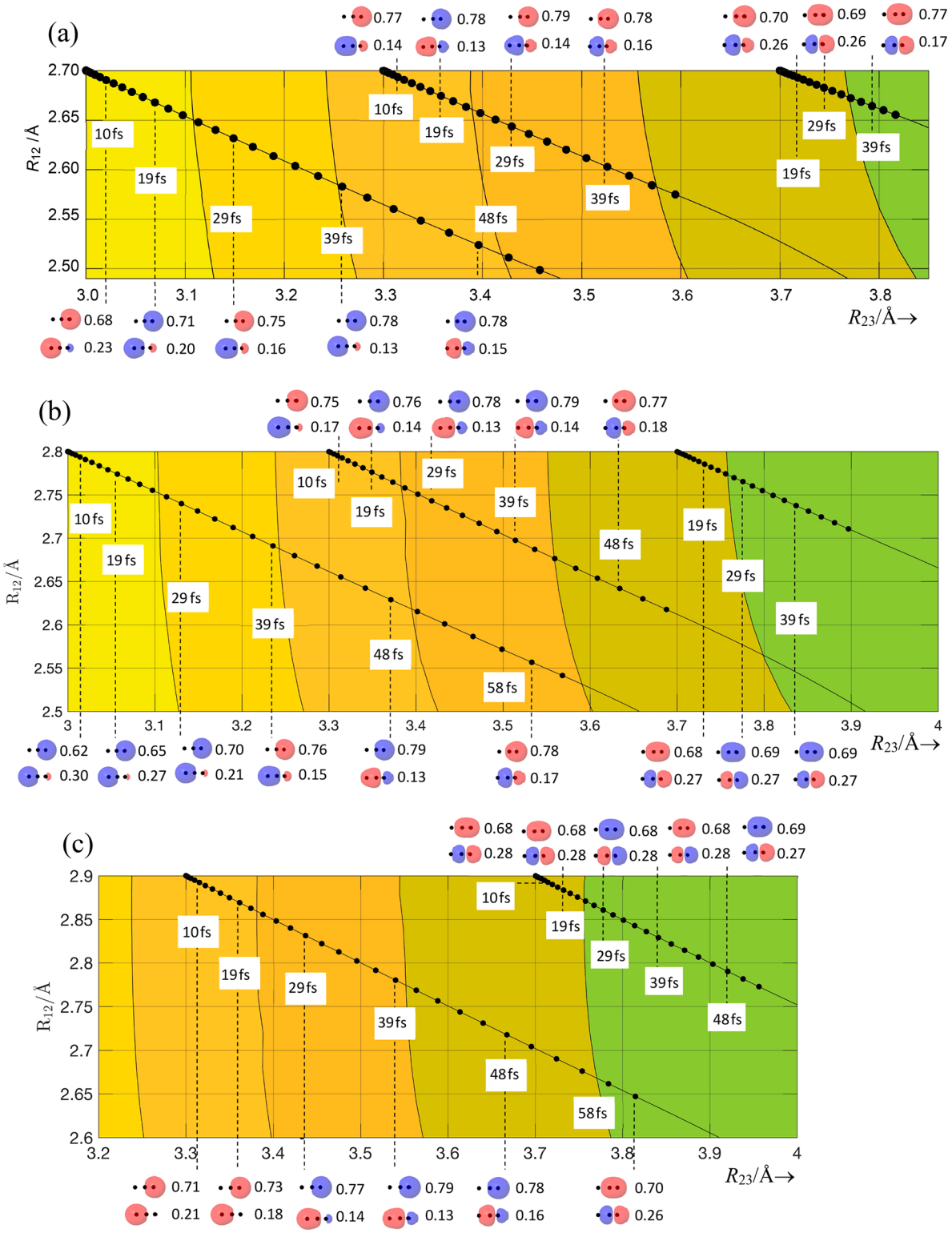

Figure 10. Representative early time trajectories. NTO entries are σ_1^2 electron orbital and σ_1^2 value above and σ_2^2 electron orbital and σ_2^2 value below. Hole orbitals are not shown. Black dots are separated by two time steps (0.1.936 fs). See Figure 8 for contour energies and text for further details.

lower adiabat along the line R_{23} = 4.00 Å. The initial ridge is followed by a flat region that drops down after encountering a ridge at R_{12} = 4.00 Å. This latter ridge runs along a line at 45° with respect to the axes. This view along R_{23} = 4.0 Å describes the black curve in Figure 9b. Figure 9c is for R_{23} = 3.50 Å. The energy at the center of the gap is 0.168 eV, the gap is 48 cm^{-1}, and R_{12} at the center of the gap is 2.30 Å.

3.3. Trajectories. Trajectories were launched on the lowest triplet PES. The stationary-atoms ansatz is in reasonable accord with the kinetic energy of liquid helium and the relatively large amount of kinetic energy that follows exciton creation. At 2 K, each He atom has, on average, about 10 cm^{-1} of kinetic energy,[59] in which case each nuclear degree of freedom has about 3 cm^{-1}. The kinetic energy is due mainly to zero-point

DOI: 10.1021/acs.jpca.9b03241
J. Phys. Chem. A 2019, 123, 6113−6122

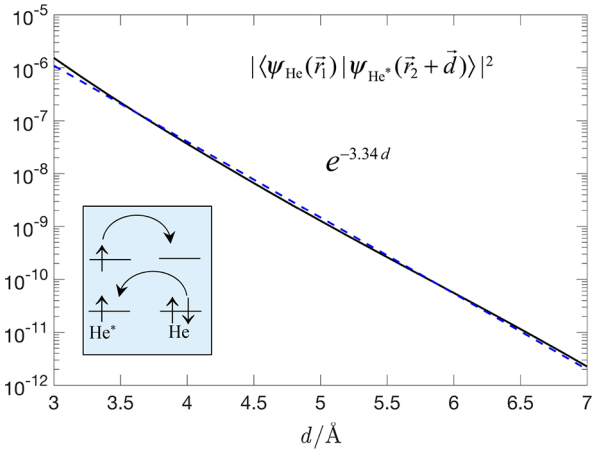

Figure 11. Squared overlap of wave functions versus separation d between nuclei. The vectors locate electrons on atoms 1 and 2. The black line shows the squared overlap; the blue dashed line is the exponential decay. For a triplet exciton to hop requires concerted electron transfer (box in lower left).

fluctuations, so the 10 cm^{-1} value changes little with temperature.

The trajectory calculations do not include nonadiabatic transitions. It is easy to see what is going on at large distances insofar as effects due to nonadiabatic transitions. Referring to Figure 9a, a trajectory propagating from small R_{12} through the near-degeneracy point will pass from the lower to the upper adiabat with essentially 100% efficiency. Indeed, staying on either adiabat as R_{12} goes from, *e.g.*, 2.20 to 2.50 Å is not an option. This would require an exciton to hop a distance that is too large to be feasible, as discussed below. This behavior was confirmed by calculating nonadiabatic couplings among the three lowest PESs as R_{12} traverses this region with R_{23} = 6.00 Å.

The role of nonadiabatic transitions is clear in extreme cases such as the large-R_{23} case discussed above. However, their roles are not obvious *a priori* for many of the R_{12}^0 and R_{23}^0 values inside the box in Figure 8. Dynamics are expected to be complicated when kinetic energies are comparable to or larger than energy differences between PESs, which arises along many trajectories. In these cases, it is possible that more than two PESs participate. For the time being, we put such complexities aside until a thorough study of nonadiabatic processes has been carried out. This will be the focus of the next generation of our calculations.

Figure 10 shows representative trajectories, including NTOs, for sufficiently early times that nonadiabatic transitions do not enter the picture. A total of 40 trajectories commenced propagation on the lower adiabat for starting distances: $2.7 \le R_{12}^0 \le 3.0$ Å and $3.0 \le R_{23}^0 \le 3.9$ Å, in steps of 0.10 Å. The above values lie within or on the rectangle in Figure 8. The sampling of these trajectories presented in Figure 10 tells the story except at and near a symmetry point. Namely, the starting point (R_{12}^0, R_{23}^0) = (3.0, 3.0) cannot break its symmetry. Atom 2 remains motionless as atoms 1 and 3 leave symmetrically. Nearby starting points: (R_{12}^0, R_{23}^0) = (3.0, 3.0), (3.0, 3.1), (3.0, 3.2), (2.9, 3.0), and (2.9, 3.1), behave similarly. However, the remaining 35 trajectories all have R_{12} decreasing and R_{23} increasing at short times.

The NTOs in Figure 10 are placed above and below panels a–c. Each NTO entry consists of the σ_1^2 value and its corresponding electron orbital above and the σ_2^2 value and its corresponding electron orbital below. Hole orbitals are not shown. They are more compact, as illustrated in Figure 9, and are localized on the same atoms as the particle orbitals along the trajectories. Times (rounded to the nearest femtosecond) are given in white boxes, with dashed lines connecting NTOs to black dots along the trajectories. The black dots are separated by two time steps (*i.e.*, one dot every 1.936 fs) and connected by thin lines to guide the eye. The NTOs show initial delocalization (*i.e.*, amplitude on all three atoms, except for the larger R_{23}^0 values). In each of the 35 trajectories, early time evolution has R_{12} decreasing and R_{23} increasing. The NTOs evolve over 10s of femtoseconds toward a diatom exciton for the smaller R_{23} values. They change rather little for the larger R_{23} values. As mentioned above, the only way to deal with trajectories at longer times is through dynamics studies that include nonadiabatic transitions among low-lying adiabats.

The excitons under consideration consist of a Rydberg electron and a hole, and concerted electron transfer must take place for the exciton to hop. In the three-atom cases, the Rydberg electron must hop from He_2* to atom 3 in concert with an electron on atom 3 moving to the He_2* hole (or a Rydberg electron on atom 3 must hop to a ground state He_2 pair in concert with an electron on the He_2 pair moving to the He* hole). To get an idea of how this varies with distance between sites, d, the squared overlap: $|\langle\psi_{He}(\vec{r}_1\psi_{He^*}(\vec{r}_2+\vec{d})\rangle|^2$ vs d is given in Figure 11. It is for He* + He → He + He*, but He_2* + He → He_2 + He* behaves similarly. Section 3.4 and the Supporting Information give examples of how failure to include nonadiabatic transitions results in unphysical hops.

Referring to Figure 9a, consider staying on the lower adiabat versus making a nonadiabatic transition to the upper adiabat when a trajectory going from left to right reaches the near degeneracy. It makes a nonadiabatic transition, because to stay on an adiabat would require the exciton to hop over too large a distance. Perusal of trajectories in this way leads to an important conclusion: Restricting dynamics to one adiabat results in unphysical hops, whereas including nonadiabatic transitions

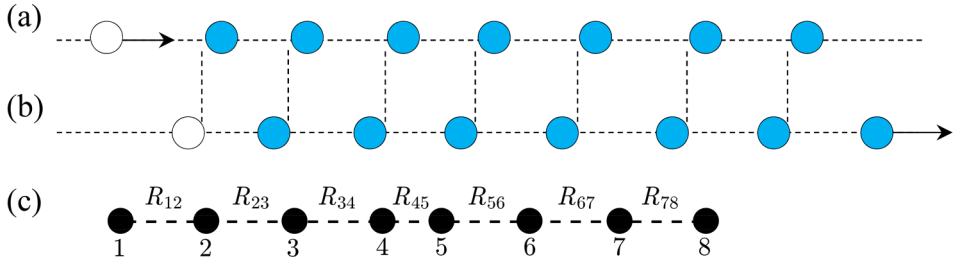

Figure 12. (a) The cue ball strikes the first of seven stationary balls. Each ball strikes the one to its right until the end. (b) The rightmost ball has the momentum. (c) This depicts eight He atoms before promotion to the lowest triplet adiabat.

DOI: 10.1021/acs.jpca.9b03241
J. Phys. Chem. A 2019, 123, 6113–6122

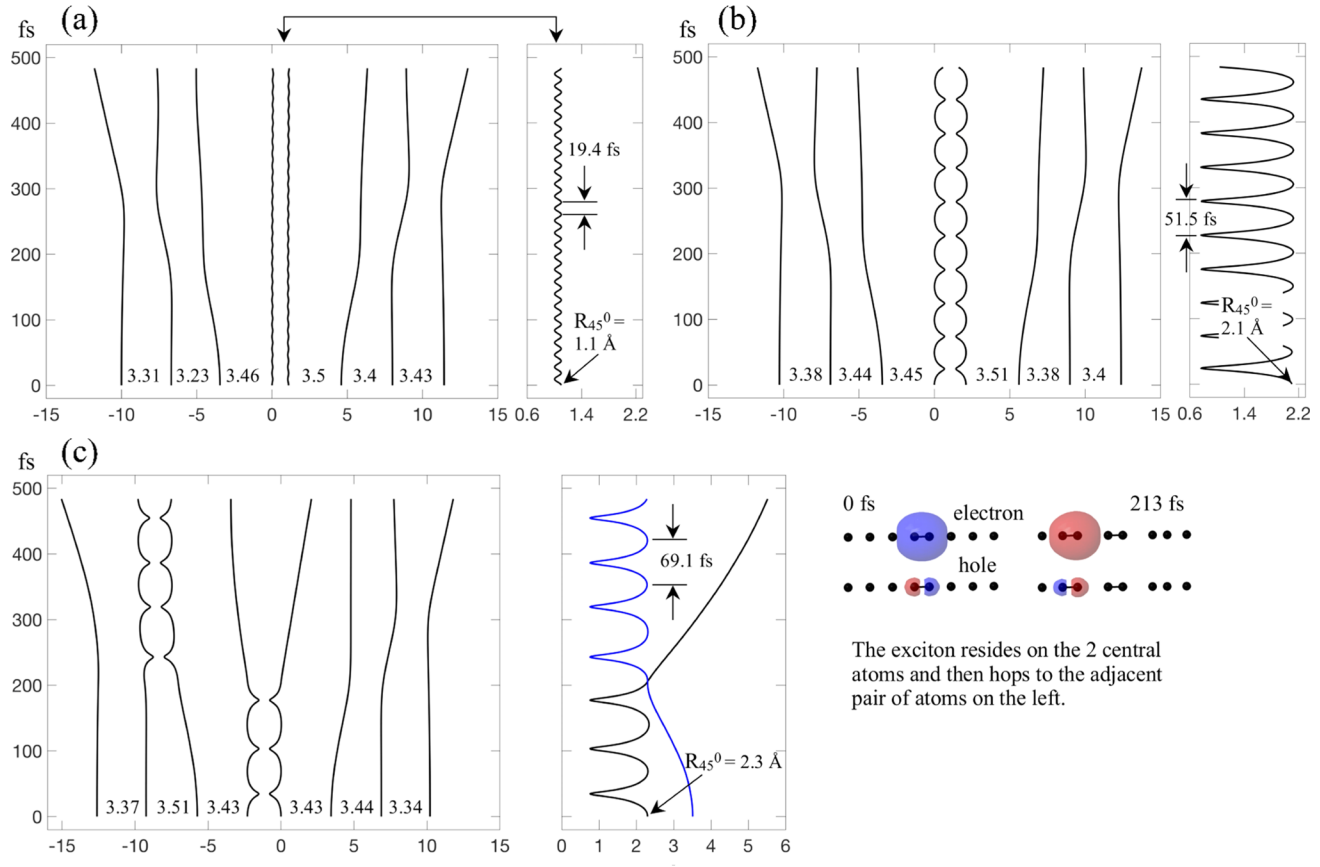

Figure 13. Collinear eight-atom systems: In (a) and (b), R_{45}^0 values of 1.10 and 2.10 Å ensure exciton oscillation *ad infinitum*. Repulsion experienced by the other atoms is similar. This is a consequence of the adiabatic separation of timescales. In (c), the 7.06 Å hop is an artifact due to the use of Born−Oppenheimer molecular dynamics. Such hops will not be present when nonadiabatic coupling is included.

eliminates them. The next section demonstrates this in collinear eight-atom clusters.

To conclude this section, note that the exciton must be on an atom when R_{12} and R_{23} are large. Alternatively, when R_{23} is large and R_{12} is not, we have the possibility of He_2* and atom 3, as well as the possibility of the exciton on atom 3 and a He_2 dimer. At large R_{23}, the lower and upper adiabats act together to yield He_2* perturbed by a distant He atom.

3.4. Eight Atoms. The game of pool is a playground for classical physics on a flat surface.[60] Consider a collinear arrangement in which a cue ball strikes one end (Figure 12a) initiating a series of collisions. Leaving aside friction, after the collisions have ceased, the ball on the far right has the same velocity as did the incident cue ball (Figure 12b). The others are stationary. The analogous arrangement of He atoms in Figure 12c will be used to illustrate a few effects, most importantly, the role of nonadiabatic transitions. Arrangements of six, seven, and nine atoms yield similar conclusions.

Parts a and b of Figure 13 show stable excitons whose initial separations are R_{45}^0 = 1.10 and 2.10 Å, respectively, with other pair distances in the range 3.23−3.51 Å. The exciton oscillations are rapid compared to the motions they engender in the other atoms. This adiabatic separation of timescales persists over a wide range of He_2* vibrational energy. Starting at t = 0, atoms 3 and 6 are repelled, causing them to move toward atoms 2 and 7, respectively. Atoms other than 3 and 6 are also repelled by the exciton, but much less. Roughly speaking, all atoms other than 4 and 5 interact with one another through potentials like the one in Figure 3 until they are overwhelmed by repulsion from the exciton. Energy propagates outward, liberating atoms 1 and 8. Note the high degree of left−right symmetry.

One gets a rough idea of the timescale for outward propagation of energy. Referring to Figure 13a, at 200 fs, atom 3 has moved 1.07 Å, the distance from the He_2* center-of-mass (CM) to atom 3 has increased from 4.01 to 5.08 Å, and R_{23} has shortened from 3.23 to 2.37 Å. Figure 2 shows He−He repulsion rising steeply there, causing R_{23} to expand. The collinear arrangement exaggerates the effectiveness of energy transfer in the same way as does the pool-ball example. Trajectories end at 484 fs with fragmentation of the original cluster yielding He_2*, two dimers, and atoms 1 and 8. The system ceased behaving as an eight-atom adiabat at ∼200 fs, because of minimal interaction between the exciton and atoms 3 and 6.

Figure 13b is for R_{45}^0 = 2.10 Å. Note that the potential energy of isolated He_2* at 2.10 Å is 14 368 cm^{-1}, which is 0.92 D_e, and the oscillation period has increased from 19.4 fs for R_{45}^0 = 1.10 Å, to 51.5 fs, and oscillation is quite anharmonic. Nonetheless, time averaged repulsion, judged by motions of the other six atoms, is like that in Figure 13a. This is because of the rapid exciton oscillation relative to the motions of the other atoms. In liquid helium there will be an outward push from an exciton on a timescale that is much longer than that over which incipient He_2* starts toward its potential energy minimum.

For R_{45}^0 = 2.30 (Figure 13c), an exciton hop appears when the distance between the R_{45} and R_{23} CMs is 7.06 Å. Even more egregious is that this happens in <1 fs. As discussed above,

DOI: 10.1021/acs.jpca.9b03241
J. Phys. Chem. A 2019, 123, 6113−6122

such exciton hops arise due to using Born−Oppenheimer molecular dynamics. A more extreme example is in the Supporting Information.

4. CONCLUSIONS

We have examined adiabatic PESs, nuclear dynamics, and timescales relevant to He_2^* formation. The timescale for ensuring creation of He_2^* moieties is smaller than that of pushing He atoms away from an exciton. The crucial role of nonadiabatic transitions in such systems has been established. Specific points are listed below.

- The presence of He_2^* following the creation of a triplet exciton in liquid helium had been puzzling, as gas-phase $He^* + He \rightarrow He_2^*$ has a barrier whose peak energy exceeds 500 cm^{-1}. This seemed insurmountable at a few Kelvin. However, He_2^* can be produced in concert with exciton creation via a few-body effect.
- The radial distribution function of liquid helium peaks at 3.5 Å and is down to half its peak value at 2.7 Å. The gas-phase $He^* + He \rightarrow He_2^*$ barrier peaks at 2.7 Å. We estimate that R_{cr} values of 2.5, 2.6, 2.7, 2.8, 2.9, and 3.0 Å have probabilities of 0.09, 0.15, 0.24, 0.34, 0.45, and 0.57, respectively. Thus, a nearest neighbor is subsumed efficiently into incipient He_2^*.
- The two lowest triplets were calculated for interatomic distances relevant to electron-impact excitation. The lower and upper adiabats act together to recover the diatomic $a^3\Sigma_u^+$ curve, underscoring the importance of nonadiabatic dynamics in such systems.
- Early time dynamics in collinear three-atom systems has been examined using classical trajectories launched on the lower PES, which is calculated on the fly. The trajectories were launched from $2.7 \leq R_{12}^0 \leq 3.0$ Å and $3.0 \leq R_{23}^0 \leq 3.9$ Å, in steps of 0.1 Å. Timing is critical: repelling nearby helium vs incipient He_2^* evolving toward the He_2^* potential energy minimum.
- Systems comprising eight collinear atoms illustrate fragmentation of the initial cluster and unphysical exciton hops that further underscore the essential role of nonadiabatic transitions.

ASSOCIATED CONTENT

Supporting Information

The Supporting Information is available free of charge on the ACS Publications website at DOI: 10.1021/acs.jpca.9b03241.

Figures showing additional views of the two lowest energy triplet adiabats of collinear three-atom He system, slices through the adiabats as well as NTOs, and the trajectory of a collinear eight-atom system (PDF)

AUTHOR INFORMATION

Corresponding Author

*E-mail: wittig@usc.edu. Phone: (213) 740-7368.

ORCID

Anna I. Krylov: 0000-0001-6788-5016
Oleg V. Prezhdo: 0000-0002-5140-7500
Andrey F. Vilesov: 0000-0002-8412-817X
Curt Wittig: 0000-0002-8426-8869

Present Address

‡ZestFinance, 1377 N. Serrano Ave., Los Angeles, CA 90027.

Notes

The authors declare no competing financial interest.

ACKNOWLEDGMENTS

This work was supported by National Science Foundation grants CHE-1900510 (P.N. and O.V.P.), Army Research Office grant W911NF-16-1-0232 (A.I.K.), a 2019 Simons Fellowship in Theoretical Physics (A.I.K.), CHE-1362535 (A.F.V.), CHE-1664990 (A.F.V.), and AST-1800591 (C.W.).

REFERENCES

(1) Sansonetti, J. E.; Martin, W. C.; Young, S. L. *Handbook of Basic Atomic Spectroscopic Data*; National Institute of Science and Technology (NIST), 2005.

(2) Pavanello, M.; Cafiero, M.; Bubin, S.; Adamowicz, L. Accurate Born-Oppenheimer Calculations of the Low-Lying $c^3\Sigma_g^+$ and $a^3\Sigma_u^+$ Excited States of Helium Dimer. *Int. J. Quantum Chem.* **2008**, *108*, 2291−2298.

(3) Focsa, C.; Bernath, P. F.; Colin, R. The Low-Lying States of He_2. *J. Mol. Spectrosc.* **1998**, *191*, 209−214.

(4) Huber, K. P.; Herzberg, G. *Molecular Spectra and Molecular Structure IV. Constants of Diatomic Molecules*; Van Nostrand Reinhold: New York, 1979.

(5) Rosenblit, M.; Jortner, J. Excess Electron Surface States on Helium Clusters. *J. Chem. Phys.* **1994**, *101*, 9982−9996.

(6) Rosenblit, M.; Jortner, J. Dynamics of the Formation of an Electron Bubble in Liquid Helium. *Phys. Rev. Lett.* **1995**, *75*, 4079−4082.

(7) Rosenblit, M.; Jortner, J. Dynamics of Excess Electron Localization in Liquid Helium and Neon. *J. Phys. Chem. A* **1997**, *101*, 751−757.

(8) Rosenblit, M.; Jortner, J. Electron Bubbles in Helium Clusters. *J. Chem. Phys.* **2006**, *124*, 194505.

(9) Maris, H. J. Electrons in Liquid Helium. *J. Phys. Soc. Jpn.* **2008**, *77*, 111008.

(10) Huang, Y.; Maris, H. Effective Mass of an Electron Bubble in Superfluid Helium-4. *J. Low Temp. Phys.* **2017**, *186*, 208−216.

(11) Kafanov, S. G.; Parshin, A. Ya.; Todoshchenko, I. A. Structure and Dynamics of the $He_2^*(a^3\Sigma_u^+)$ Molecular Complex in Condensed Phases of Helium. *J. Exp. Theor. Phys.* **2000**, *91*, 991−999.

(12) Eloranta, J.; Apkarian, V. A. The Triplet He_2^* Rydberg States and Their Interaction Potentials with Ground State He Atoms. *J. Chem. Phys.* **2001**, *115*, 752−760.

(13) Eloranta, J.; Schwentner, N.; Apkarian, V. A. Structure and Energetics of He_2^* Bubble-States in Superfluid ^4He. *J. Chem. Phys.* **2002**, *116*, 4039−4053.

(14) Fiedler, S. L.; Eloranta, J. Interaction of Helium Rydberg State Atoms with Superfluid Helium. *J. Low Temp. Phys.* **2014**, *174*, 269−283.

(15) Hill, J. C.; Heybey, O.; Walters, G. K. Evidence of Metastable Atomic and Molecular Bubble States in Electron-Bombarded Superfluid Liquid Helium. *Phys. Rev. Lett.* **1971**, *26*, 1213−1216.

(16) Keto, J. W.; Stockton, M.; Fitzsimmons, W. A. Dynamics of Atomic and Molecular Metastable States Produced in Electron-Bombarded Superfluid-Helium. *Phys. Rev. Lett.* **1972**, *28*, 792−795.

(17) Keto, J. W.; Soley, F. J.; Stockton, M.; Fitzsimmons, W. A. Dynamic Properties of Neutral Excitations Produced in Electron-Bombarded Superfluid-Helium. 2. Afterglow Fluorescence of Excited Helium Molecules. *Phys. Rev. A: At., Mol., Opt. Phys.* **1974**, *10*, 887−896.

(18) Keto, J. W.; Soley, F. J.; Stockton, M.; Fitzsimmons, W. A. Dynamic Properties of Neutral Excitations Produced in Electron-Bombarded Superfluid-Helium. 1. $He(2^3S)$ and $He_2(a^3\Sigma)$ Atomic and Molecular Metastable States. *Phys. Rev. A: At., Mol., Opt. Phys.* **1974**, *10*, 872−886.

(19) Nijjar, P.; Krylov, A. I.; Prezhdo, O. V.; Vilesov, A. F.; Wittig, C. Conversion of $He(2^3S)$ to $He_2(a^3\Sigma_u^+)$ in Liquid Helium. *J. Phys. Chem. Lett.* **2018**, *9*, 6017−6023.

DOI: 10.1021/acs.jpca.9b03241
J. Phys. Chem. A 2019, 123, 6113−6122

(20) Gspann, J.; Vollmar, H. Metastable Excitations of Large Clusters of ^{3}He, ^{4}He or Ne Atoms. *J. Chem. Phys.* **1980**, *73*, 1657−1664.
(21) Gspann, J. Electron-Impact on Helium Clusters − Metastable Excitation, Ionization, and Charged Mini-Cluster Ejection. *Surf. Sci.* **1981**, *106*, 219−224.
(22) Gspann, J.; Vollmar, H. Ejection of Positive Cluster Ions from Large Electron-Bombarded ^{3}He or ^{4}He Clusters. *J. Low Temp. Phys.* **1981**, *45*, 343−355.
(23) Buchenau, H.; Knuth, E. L.; Northby, J.; Toennies, J. P.; Winkler, C. Mass-Spectra and Time-of-Flight Distributions of Helium Cluster Beams. *J. Chem. Phys.* **1990**, *92*, 6875−6889.
(24) Buchenau, H.; Toennies, J. P.; Northby, J. A. Excitation and Ionization of ^{4}He Clusters by Electrons. *J. Chem. Phys.* **1991**, *95*, 8134−8148.
(25) von Issendorff, B.; Haberland, H.; Frochtenicht, R.; Toennies, J. P. Spectroscopic Observation of a Metastable Electronically Excited He_4^+. *Chem. Phys. Lett.* **1995**, *233*, 23−27.
(26) Toennies, J. P.; Vilesov, A. F. Superfluid Helium Droplets: A Uniquely Cold Nanomatrix for Molecules and Molecular Complexes. *Angew. Chem., Int. Ed.* **2004**, *43*, 2622−2648.
(27) Schöbel, H.; Bartl, P.; Leidlmair, C.; Denifl, S.; Echt, O.; Märk, T. D.; Scheier, P. High-Resolution Mass Spectrometric Study of Pure Helium Droplets, and Droplets Doped with Krypton. *Eur. Phys. J. D* **2011**, *63*, 209−214.
(28) Gomez, L. F.; Loginov, E.; Sliter, R.; Vilesov, A. F. Sizes of Large He Droplets. *J. Chem. Phys.* **2011**, *135*, 154201.
(29) Tanyag, R. M.; Jones, C. F.; Bernando, C.; O'Connell, S. M. O.; Verma, D.; Vilesov, A. F. Experiments with Large Superfluid Helium Nanodroplets. In *Cold Chemistry: Molecular Scattering and Reactivity Near Absolute Zero*; Osterwalder, A., Dulieu, O., Eds.; Royal Society of Chemistry: Cambridge, 2017; pp 389−443.
(30) Fine, J.; Verma, D.; Jones, C. F.; Wittig, C.; Vilesov, A. F. Formation of He_4^+ via Electron Impact of Helium Droplets. *J. Chem. Phys.* **2018**, *148*, No. 044302.
(31) Surko, C. M.; Dick, G. J.; Reif, F. Spectroscopic Study of Liquid Helium in the Vacuum Ultraviolet. *Phys. Rev. Lett.* **1969**, *23*, 842−845.
(32) Tokaryk, D. W.; Brooks, R. L.; Hunt, J. L. Reaction Dynamics of Metastable Helium Molecules and Atoms near 4.2 K. *Phys. Rev. A: At., Mol., Opt. Phys.* **1993**, *48*, 364−381.
(33) Knowles, P. J.; Murrell, J. N. The Metastable Quartet State of He_4^+. *J. Chem. Phys.* **1995**, *102*, 9442−9443.
(34) Knowles, P. J.; Murrell, J. N. The Structures and Stabilities of Helium Cluster Ions. *Mol. Phys.* **1996**, *87*, 827−833.
(35) Müller, M. W.; Bussert, W.; Ruf, M. W.; Hotop, H.; Meyer, W. New Oscillatory Structure in Electron-Energy Spectra from Auto-ionizing Quasi-Molecules − Subthermal Collisions of He(2^3S) Atoms with He(2^1S, 2^3S) Atoms. *Phys. Rev. Lett.* **1987**, *59*, 2279−2282.
(36) Müller, M. W.; Merz, A.; Ruf, M. W.; Hotop, H.; Meyer, W.; Movre, M. Experimental and Theoretical Studies of the Bi-Excited Collision Systems He(2^3S) + He(2^3S, 2^1S) at Thermal and Subthermal Kinetic Energies. *Z. Phys. D: At., Mol. Clusters* **1991**, *21*, 89−112.
(37) Brooks, R. L.; Hunt, J. L.; Tokaryk, D. W. Absorption Spectra from High Vibrational Levels of He_2. *J. Chem. Phys.* **1989**, *91*, 7408−7414.
(38) Costa, E. D.; Lemes, N. H. T.; Braga, J. P. Accurate Potential Energy Curve for Helium Dimer Retrieved from Viscosity Coefficient Data at Very Low Temperatures. *Phys. A* **2017**, *487*, 32−39.
(39) Varandas, A. J. C. Extrapolation to the Complete Basis Set Limit Without Counterpoise. *J. Phys. Chem. A* **2010**, *114*, 8505−8516.
(40) Li, X.; Tang, M. L. Triplet Transport in Thin Films: Fundamentals and Applications (Feature Article). *Chem. Commun.* **2017**, *53*, 4429−4440.
(41) Agranovich, V. M. *Excitations in Organic Solids*; International Series of Monographs on Physics; Oxford University Press: Oxford, U.K., 2009; Vol. *142*.
(42) Shao, Y.; Gan, Z.; Epifanovsky, E.; Gilbert, A. T.; Wormit, M.; Kussmann, J.; Lange, A. W.; Behn, A.; Deng, J.; Feng, X.; et al. Advances in Molecular Quantum Chemistry Contained in the Q-Chem 4 Program Package. *Mol. Phys.* **2015**, *113*, 184−215.
(43) Krylov, A. I.; Gill, P. M. W. Q-Chem: An Engine for Innovation. *WIREs Comput. Mol. Sci.* **2013**, *3*, 317−326.
(44) Gilbert, A. T. B. IQmol molecular viewer, http://iqmol.org.
(45) Jmol: an open-source Java viewer for chemical structures in 3D. http://www.jmol.org/.
(46) Bartlett, R. J. Coupled-Cluster Theory and its Equation-of-Motion Extensions. *Wiley Interdiscip. Rev. Comput. Mol. Sci.* **2012**, *2*, 126−138.
(47) Krylov, A. I. Equation-of-Motion Coupled Cluster Methods for Open-Shell and Electronically Excited Species: The Hitchhiker's Guide to Fock Space. *Annu. Rev. Phys. Chem.* **2008**, *59*, 433−462.
(48) Yarkony, D. R. On the Quenching of Helium 2^3S − Potential-Energy Curves for, and Nonadiabatic, Relativistic, and Radiative Couplings Between, the $a^3\Sigma_u^+$, $A^1\Sigma_u^+$, $b^3\Pi_g$, $B^1\Pi_g$, $c^3\Sigma_g^+$, and $C^1\Sigma_g^+$ States of He_2. *J. Chem. Phys.* **1989**, *90*, 7164−7175.
(49) Luzanov, A. V.; Sukhorukov, A. A.; Umanskii, V. E. Application of Transition Density Matrix for Analysis of the Excited States. *Theor. Exp. Chem.* **1976**, *10*, 354−361.
(50) Mewes, S. A.; Plasser, F.; Krylov, A.; Dreuw, A. Benchmarking Excited-State Calculations Using Exciton Properties. *J. Chem. Theory Comput.* **2018**, *14*, 710−725.
(51) Plasser, F.; Wormit, M.; Dreuw, A. New Tools for the Systematic Analysis and Visualization of Electronic Excitations. I. Formalism. *J. Chem. Phys.* **2014**, *141*, 024106.
(52) Tuckerman, M. E. Ab Initio Molecular Dynamics: Basic Concepts, Current Trends, and Novel Applications. *J. Phys.: Condens. Matter* **2002**, *14*, R1297.
(53) Hockney, R. W.; Eastwood, J. W. *Computer Simulations Using Particles*; McGraw-Hill: New York, 1981.
(54) Vinen, W. F. CAS-CERN Accelerator School on Superconductivity and Cryogenics for Accelerators and Detectors 2002; pp 363−373, DOI: DOI: 10.5170/CERN-2004-008.363.
(55) Ceperley, D. M. Path-Integrals in the Theory of Condensed Helium. *Rev. Mod. Phys.* **1995**, *67*, 279−355.
(56) Svensson, E. C.; Sears, V. F.; Woods, A. D. B.; Martel, P. Neutron-Diffraction Study of the Static Structure Factor and Pair Correlations in Liquid ^{4}He. *Phys. Rev. B: Condens. Matter Mater. Phys.* **1980**, *21*, 3638−3651.
(57) Robkoff, H. N.; Hallock, R. B. Structure-Factor Measurements in ^{4}He at Saturated Vapor-Pressure for 1.38 < T < 4.24 K. *Phys. Rev. B: Condens. Matter Mater. Phys.* **1981**, *24*, 159−182.
(58) McQuarrie, D. A. *Statistical Mechanics*; University Science Books: Sausalito, CA, 2000; Chapter 13.
(59) Boninsegni, M. Kinetic Energy and Momentum Distribution of Isotopic Liquid Helium Mixtures. *J. Chem. Phys.* **2018**, *148*, 102308.
(60) Shepard, R.*Amateur Physics for the Amateur Pool Player*; 1997; https://www.tcbilliards.com/articles/physics.shtml

DOI: 10.1021/acs.jpca.9b03241
J. Phys. Chem. A 2019, 123, 6113−6122